Biomolecules and Biomedicine
ISSN: 2831-0896 (Print) | ISSN: 2831-090X (Online)
Journal Impact Factor® (2025): 2.8
CiteScore® (2025): 4.7
www.biomolbiomed.com | blog.bjbms.org

The BiomolBiomed publishes an "Advanced Online" manuscript format as a free service to authors in order to expedite the dissemination of scientific findings to the research community as soon as possible after acceptance following peer review and corresponding modification (where appropriate). An "Advanced Online" manuscript is published online prior to copyediting, formatting for publication and author proofreading, but is nonetheless fully citable through its Digital Object Identifier (doi®). Nevertheless, this "Advanced Online" version is NOT the final version of the manuscript. When the final version of this paper is published within a definitive issue of the journal with copyediting, full pagination, etc., the new final version will be accessible through the same doi and this "Advanced Online" version of the paper will disappear.

RESEARCH ARTICLE

Zhang et al.: GATA2/IER3 in breast cancer

GATA2-mediated IER3 transcription promotes breast cancer progression and tumor-associated immunosuppression

Jiazhennan Zhang[1], Qian Zhao[2], Dan Li[2], Yuxiang Li[2], Dilixiati Jinsihan[2*]

[1]Phase I Clinical Trial Unit, Affiliated Tumor Hospital, Xinjiang Medical University, Urumqi, China;

[2]Department of Breast Surgery, Affiliated Tumor Hospital, Xinjiang Medical University, Urumqi, China.

*Correspondence to **Dilixiati Jinsihan**: dixt716@126.com.

DOI: https://doi.org/10.17305/bb.2026.14970

EARLY ACCESS

ABSTRACT

The molecular mechanisms linking breast cancer (BC) progression to an immunosuppressive tumor microenvironment remain incompletely understood. We investigated the role of the GATA2/IER3 axis in BC progression and immune-related cellular responses. Bulk transcriptomic datasets GSE10810 and GSE42568 and the single-cell RNA sequencing dataset GSE161529 were integrated with immune-related gene lists. Support vector machine-recursive feature elimination, The Cancer Genome Atlas data, and immune-infiltration analyses prioritized candidate genes. Expression was evaluated in BC tissues and cell lines. Knockdown and rescue experiments assessed BC cell proliferation, apoptosis, migration, and invasion, together with $CD8^+$ T-cell responses and macrophage markers in coculture. Chromatin immunoprecipitation-qPCR and dual-luciferase reporter assays examined transcriptional regulation, and nude mouse xenografts assessed tumor growth. Immediate early response 3 (IER3) was upregulated in BC tissues and cells and was associated with an immunosuppressive infiltration profile. IER3 knockdown inhibited BC cell proliferation, migration, and invasion and increased apoptosis. It also enhanced $CD8^+$ T-cell proliferation and interferon-γ secretion, reduced T-cell apoptosis, and decreased the proportion of CD206-positive macrophages. GATA binding protein 2 (GATA2) bound to the IER3 promoter and activated transcription. IER3 overexpression partially reversed the effects of GATA2 knockdown on BC cells and cocultured immune cells. *In vivo*, GATA2 knockdown reduced tumor growth, increased CD86 staining, and decreased CD206 staining; IER3 overexpression partially attenuated these effects (all $p < 0.05$). These findings support a role for GATA2-mediated IER3 transcription in BC progression and immune-related cellular responses. Its effects on adaptive antitumor immunity *in vivo* require further investigation.

Keywords: Breast cancer, GATA2, IER3, immune suppression, single-cell RNA sequencing, tumor immune microenvironment, macrophage polarization.

EARLY ACCESS

INTRODUCTION

Among women globally, breast cancer (BC) represents one of the prevalent malignant diseases and serves as a primary driver of cancer deaths [1–3]. In spite of notable improvements in radiotherapy, chemotherapy, and targeted agents during the last several decades, patients with metastatic or advanced BC still face an unfavorable clinical outcome [4, 5]. Tumor recurrence, metastasis, and treatment resistance continue to represent major clinical challenges affecting long-term survival [6, 7]. The advent of immune checkpoint inhibitors has broadened the therapeutic options for BC and have demonstrated clinical value, particularly in triple-negative BC. However, only a subset of patients achieves durable therapeutic responses [8–10]. Multiple accumulating studies have proven unsatisfactory immunotherapeutic outcomes for BC rely on both cell-autonomous molecular properties of neoplastic cells and the immune-inhibitory tumor microenvironment (TME) [11–13]. Therefore, clarifying molecular signaling cascades behind oncogenic advancement of BC cells and their remodeling of the immune microenvironment is important for identifying new therapeutic targets.

Critically involved in BC growth, invasion, metastasis, and treatment resistance, the TME is composed of various cytokines [14–16]. $CD8^+$ T cells are major effectors of antitumor immunity and eliminate tumor cells by sensing tumor antigens and discharging cytotoxic effectors, including perforin and granzymes [17, 18]. In patients with BC, the level of $CD8^+$ T-cell infiltration, their spatial organization, and functional competence strongly associate with response to therapy and overall prognosis [19, 20]. Macrophages associated with tumors (TAMs) represent a key immune subset in the TME and exhibit considerable phenotypic and functional plasticity [21, 22]. M1-like macrophages generally participate in proinflammatory and antitumor immune responses, whereas M2-like macrophages promote angiogenesis, invasion, and contribute to metastasis via secretion of immunosuppressive cytokines and growth factors. M2-like macrophages can also suppress the recruitment, activation, and cytotoxic activity of $CD8^+$ T cells [23–25]. The immunosuppressive state characterized by increased M2-like macrophages, impaired $CD8^+$ T-cell function, and spatial exclusion of $CD8^+$ T cells provides an important basis for immune escape and treatment resistance in BC [26]. However, the tumor-intrinsic molecular mechanisms through which BC cells simultaneously regulate macrophage polarization

EARLY ACCESS

and $CD8^+$ T-cell function remain incompletely understood. Therefore, elucidating the molecular regulatory network between BC cells and immune cells is essential for understanding BC progression and developing new therapeutic strategies.

In recent years, advances in high-throughput transcriptomic technologies have provided important opportunities for the systematic identification of disease-related candidate genes using publicly available datasets. Bulk transcriptomic analysis is capable of revealing altered gene expression, whereas single-cell RNA sequencing (scRNA-seq) enables the characterization of cellular composition, heterogeneity, and cell type-specific expression patterns within tumor tissues at single-cell resolution, as well as the identification of cellular subpopulations with distinct biological characteristics and functions [27–29]. scRNA-seq is now widely employed in BC research and provides an important approach for elucidating cellular diversity within the TME, tumor cell states, and their dynamic changes [30, 31]. Therefore, leveraging both bulk transcriptomic information and scRNA-seq data may facilitate the detection of genes that are pivotal for BC progression and the immune microenvironment.

Based on this background, the present study integrated public bulk transcriptomic and scRNA-seq data for the discovery of key genes relevant to BC progression and the immune microenvironment and to examine their potential contributions. Functional experiments and immune cell co-culture systems were subsequently employed to assess the impact of the key gene on the malignant biological properties of BC cells, $CD8^+$ T-cell function, and macrophage polarization, and to clarify the fundamental molecular mechanism. The main objective of this work was to investigate the molecular relationship between BC progression and immune microenvironment-related changes and to provide a basis for further investigation of the GATA2/IER3 axis.

MATERIALS AND METHODS

Public datasets and differential expression analysis

Raw transcriptional profiles corresponding to accession numbers GSE10810 and GSE42568 were acquired via the public Gene Expression Omnibus (GEO) platform (https://www.ncbi.nlm.nih.gov/geo/). The former dataset covers 31 BC tissue samples and 27 non-tumor breast tissues, while the latter consists of 104 malignant breast specimens and 17 normal controls. Differentially expressed genes (DEGs) were screened from the GSE10810 and GSE42568 cohorts by differential expression

analysis with limma (v3.62.2), where significance thresholds were set as |log2fold change (FC)| > 1.0 and adjusted $p < 0.05$. Multiple comparison correction was carried out with the Benjamini–Hochberg method, yielding adjusted p values. The R package ggplot2 served to create volcano plots illustrating the overall pattern of DEGs. The ImmPort platform (https://www.immport.org/) and MSigDB resource (https://www.gsea-msigdb.org/gsea/msigdb/) supplied all immune-relevant genes for subsequent analysis. The overlapping genes between immune-related genes (IRGs) and DEGs from the two BC cohorts (GSE10810 and GSE42568) were identified using Venn analysis and defined as GEO-derived immune-related candidates (GEO-IRGs).

Single-cell RNA sequencing (scRNA-seq) data processing

The scRNA-seq dataset GSE161529, comprising 24 normal breast tissues and 45 BC tissues, was downloaded from GEO. Data were processed using Seurat (version 5). Exclusion criteria included cells with over 5,000 expressed genes, over 20,000 UMIs, more than 25% mitochondrial transcripts, and at least 1% hemoglobin transcripts. Gene features detected in fewer than three cells were filtered out, and doublets were detected and excluded on a per-sample basis using scDblFinder. After quality control, 305,190 cells and 26,626 genes were retained for subsequent analysis. Raw single-cell expression matrices underwent normalization via the LogNormalize function at a scaling factor of 10,000. Genes with the top 2,000 variance ranks were extracted following the vst calculation approach. Principal component analysis was performed, followed by Harmony integration for batch-effect correction using dims = 1:20, theta = 2, and lambda = 1. Leiden clustering was performed on the Harmony-corrected embeddings (algorithm = 4, resolution = 0.5). Uniform manifold approximation and projection (UMAP) was conducted with n.neighbors = 30 and min.dist = 0.1. Cell types were annotated using a combination of SingleR, DotPlot validation with literature-derived marker genes, and manual cluster-to-cell-type mapping. The tumor and normal sample identities were assigned according to the original annotations provided in the GEO dataset. Seven major cell populations were identified. For B cells, macrophages, T cells, and epithelial cells, the Seurat FindMarkers function (Wilcoxon rank-sum test) was employed to perform exploratory differential expression analysis between BC and normal cells. Considering the non-independence of cells derived from the same patient, these cell-level differential expression results

EARLY ACCESS

were interpreted as exploratory evidence for candidate gene screening rather than patient-level statistical inference. After Benjamini–Hochberg adjustment, the threshold for significance was set at $|\log2FC| > 0.26$ and adjusted $p < 0.05$. The DEGs shared by the four cell types were defined as shared scRNA-seq DEGs (SC-DEGs) to identify transcriptional alterations common across multiple TME-associated cell populations. The SC-DEGs were further intersected with IRGs to obtain single-cell-derived immune-related candidates (SC-IRGs), which were then integrated with GEO-IRGs to identify candidate genes.

Machine learning, external validation, and immune infiltration analysis

The overlapping candidate genes identified by integrating GEO-derived immune-related candidates and single-cell-derived immune-related candidates were further prioritized using support vector machine-recursive feature elimination (SVM-RFE) in the GSE42568 dataset with the R package "e1071." The five overlapping candidate genes were used as input features. The SVM-RFE algorithm was performed by recursively eliminating features, and different feature combinations were evaluated through cross-validation. The optimal gene combination was selected based on the highest classification performance. Boxplots were generated using the R package "ggplot2" to compare candidate gene expression between BC and normal tissues in the GSE10810, GSE42568, and TCGA-BRCA datasets. These datasets were used for independent validation of candidate gene expression patterns. The Genomic Data Commons portal (https://portal.gdc.cancer.gov/) supplied all raw TCGA-BRCA sequencing profiles for downstream analysis. Intergroup expression discrepancies were assessed with the Wilcoxon rank-sum analytical approach. To examine the relationships between key gene expression and the inferred infiltration levels of B cells, $CD8^+$ T cells, M1 macrophages, and M2 macrophages, TIMER2.0 (https://timer.cistrome.org/) was applied. Correlation scatterplots were subsequently generated. Statistical significance was defined whenever the corresponding p value fell below 0.05. The processed gene lists generated during the computational screening procedure are provided in the supplementary materials (Supplementary Excel file: "Processed gene lists").

Clinical specimen collection

Paired BC and adjacent non-tumor specimens from 63 patients who underwent surgical resection at Affiliated Tumor Hospital, Xinjiang Medical University were

EARLY ACCESS

obtained, pathologically verified, immediately snap-frozen in liquid nitrogen, and preserved at −80 °C until use.

Cell culture

The human normal mammary epithelial cell line MCF-10A, BC lines MCF-7 and MDA-MB-231, and the monocytic line THP-1 were purchased from Procell (Wuhan, China). Growth medium for MCF-7 and MDA-MB-231 cells consisted of DMEM (Solarbio, Beijing, China) supplemented with 10% fetal bovine serum (Gibco) and 1% antibiotic–antimycotic (penicillin–streptomycin, Gibco). RPMI-1640 medium (Solarbio) with 10% FBS and 1% penicillin–streptomycin served for THP-1 cell culture. MCF-10A cells were propagated in DMEM/F12 containing 5% horse serum, EGF, hydrocortisone, cholera toxin, insulin, and 1% penicillin/streptomycin. Cultures were maintained at 37 °C under a humidified 5% CO_2 atmosphere. Each line was authenticated via short tandem repeat (STR) profiling and confirmed mycoplasma-free before use. For THP-1 cells, exposure to 100 ng/mL PMA (Solarbio) over 24 h was used to trigger M0-like macrophage differentiation.

Cell transfection

Short hairpin RNA plasmids targeting immediate early response 3 (IER3) and GATA binding protein 2 (GATA2) (sh-IER3 and sh-GATA2) and the corresponding negative control plasmid (sh-NC) were constructed by GeneChem (Shanghai, China). The IER3 overexpression plasmid (oe-IER3) or GATA2 overexpression plasmid (oe-GATA2) were generated by cloning the full-length coding sequence of IER3 or GATA2 into the pcDNA3.1 vector (Invitrogen, Carlsbad, CA, USA), with the corresponding empty vector (Vector) used as the negative control. Transfection and co-transfection of cells were carried out using Lipofectamine 3000 (Invitrogen).

RNA extraction and reverse transcription-quantitative PCR

RNAiso Plus extraction reagent (TaKaRa, Kusatsu, Japan) was adopted to isolate total cellular RNA. The PrimeScript RT Reagent Kit manufactured by TaKaRa facilitated reverse transcription of purified RNA templates to complementary DNA (cDNA). Subsequent RT-qPCR reactions utilized TB Green Premix Ex Taq II (TaKaRa), with GAPDH as the internal control. Relative expression values were obtained using the $2^{-\Delta\Delta Ct}$ calculation, and primer sequences appear in Table 1.

EARLY ACCESS

Western blot

Whole cellular and tissue protein contents of BC samples were harvested with chilled RIPA lysis buffer manufactured by Beyotime (Shanghai, China). Once protein concentration calibrations finished, identical protein masses were resolved via 10% SDS-PAGE electrophoresis, followed by transmembrane transfer to polyvinylidene fluoride membranes from Millipore (Burlington, MA, USA). Blocking was carried out with 5% non-fat milk (Beyotime) in TBST for 1.5 h at ambient temperature. Afterwards, membranes were incubated overnight at 4 °C with antibodies against IER3 (1:1000, ab65152, Abcam, Cambridge, UK), GATA2 (1:1000, ab109241, Abcam), or β-actin (1:1000, ab8227, Abcam). After rinsing, membranes underwent 1 h incubation at ambient temperature with HRP-linked secondary antibody (1:2000, ab6721, Abcam). Subsequently, an ECL kit (Invitrogen) was used to develop the protein bands. Finally, band optical densities were analyzed with ImageJ, and the levels of target proteins were calculated relative to β-actin.

Colony formation assay

Following treatment, BC cells, seeded at 500 cells per well in 6-well plates, were cultured over a 14-day period, during which the medium was refreshed every 3 days. The colonies were washed with PBS, fixed with 4% paraformaldehyde (Solarbio) for 15 min, and stained with 0.1% crystal violet (Solarbio) for 30 min at room temperature. Cell colonies with no fewer than 50 cells were enumerated, after rinsing and air-drying, using an inverted optical microscope.

Flow cytometry analysis of apoptosis

Apoptosis was detected using an Annexin V-FITC Apoptosis Detection Kit (Beyotime) following the manufacturer's directions. Post-treatment MCF-7 and MDA-MB-231 cell suspensions were harvested, subjected to two rounds of PBS cleansing, and diluted in 500 μL binding buffer for staining preparation. Supplementary staining reagents including 5 μL Annexin V-FITC and 5 μL propidium iodide (PI) were introduced to the cell suspension sequentially. Dark incubation lasting 15 min at ambient temperature was conducted ahead of cellular detection via flow cytometric equipment.

EARLY ACCESS

Wound-healing assay

After seeding BC cells into 6-well plates and allowing them to reach full confluence, a linear defect was made with a sterile 200-μL pipette tip. The wells were then washed with PBS to eliminate dislodged cells, followed by incubation in medium without serum. With an inverted microscope, photographs of the identical scratch areas were obtained at 0 h and 24 h. Wound widths were measured using ImageJ software, and the cell migration rate was calculated.

Transwell invasion assay

Cell invasion was examined using 24-well Transwell chambers (8-μm pore size, Corning, NY, USA) that had been coated with Matrigel beforehand. Into the upper chamber, 5×10^4 treated cells resuspended in 200 μL of serum-free medium were introduced, while the lower chamber was supplied with 600 μL of medium plus 10% FBS. Cells that had not invaded and remained on the upper membrane surface were gently wiped off with a cotton swab following a 24-h incubation at 37 °C. Those that had penetrated the membrane were subjected to 15-min fixation with 4% paraformaldehyde and 20-min staining with 0.1% crystal violet at ambient temperature. After drying in air and rinsing, each insert was examined under an inverted microscope. Invading cells were then enumerated in five random fields per well.

Isolation, activation, and co-culture of $CD8^+$ T cells

Density-gradient centrifugation with Ficoll-Paque PLUS (GE Healthcare, Chicago, IL, USA) was employed to isolate peripheral blood mononuclear cells (PBMCs) from three healthy donors. $CD8^+$ T cells were subsequently purified by negative magnetic selection using a human $CD8^+$ T Cell Isolation Kit (Miltenyi Biotec, Bergisch Gladbach, Germany). The purity of the isolated $CD8^+$ T cells was assessed by flow cytometry based on CD3 and CD8 expression and was greater than 95%. Cells obtained from each donor were analyzed independently. The isolated $CD8^+$ T cells were cultured in complete RPMI-1640 medium supplemented with 100 IU/mL recombinant human interleukin-2 (IL-2) and activated using plate-bound anti-CD3 antibody (5 μg/mL) and soluble anti-CD28 antibody (2 μg/mL, BioLegend, San Diego, CA, USA). After 48 h of co-culture (effector:target = 1:1) between activated $CD8^+$ T cells and treated MCF-7 or MDA-MB-231 cells, supernatants were obtained, centrifuged at 300 × g for 5 min, and stored at −80 °C. A human interferon-gamma

(IFN-γ) ELISA kit (Thermo Fisher Scientific, Waltham, MA, USA) served to quantify IFN-γ in the supernatants, with absorbance measured at 450 nm. For apoptosis evaluation, non-adherent $CD8^+$ T cells recovered after co-culture were stained with the Annexin V-FITC/PI kit and analyzed via flow cytometry. For flow-cytometric analysis, lymphocytes were first identified according to forward- and side-scatter characteristics, followed by singlet gating based on FSC-A and FSC-H. The $CD3^+CD8^+$ population was then selected, and Annexin V-FITC/PI staining was analyzed within this population.

Carboxyfluorescein succinimidyl ester (CFSE) proliferation assay

$CD8^+$ T-cell proliferation was evaluated using a CFSE Cell Proliferation and Cytotoxicity Assay Kit (Beyotime). Briefly, $CD8^+$ T cells were labeled with CFSE for 15 min. After washing, cells were suspended in fresh RPMI-1640 complete medium and then co-incubated with transfected MCF-7 or MDA-MB-231 cells (effector: target = 1:1) over a 48-h period. $CD8^+$ T cells were subsequently collected, and cell proliferation was determined by analyzing CFSE fluorescence dilution using flow cytometry.

Flow-cytometric analysis of macrophage polarization

THP-1 cells were treated with phorbol 12-myristate 13-acetate (PMA, 100 ng/mL, Beyotime) for 24 h to induce differentiation into M0-like macrophages and were then maintained in fresh PMA-free medium for an additional 24 h. M0-like macrophages were seeded in the lower chambers of 0.4-μm Transwell plates, whereas transfected MCF-7 or MDA-MB-231 cells were seeded in the upper inserts. The two cell types were co-cultured for 48 h using a 1:1 seeding ratio. After co-culture, macrophages were collected and incubated with PE-conjugated anti-CD86 antibody (ab77226, abcam) and APC-conjugated anti-CD206 antibody (ab326477, abcam) for 30 min at 4 °C in the dark. After being washed twice in PBS, the cells underwent flow cytometric analysis, and FlowJo was used for data processing. Macrophages were first identified according to forward- and side-scatter characteristics, followed by singlet gating based on FSC-A and FSC-H. Unstained and single-stained controls were used for fluorescence compensation and gate placement. The percentages of CD86-positive and CD206-positive cells were used to evaluate M1-like and M2-like polarization, respectively.

EARLY ACCESS

Chromatin immunoprecipitation assay (ChIP)

Millipore's ChIP detection kit (Billerica, MA, USA) served as the experimental tool for chromatin immunoprecipitation in line with product guidelines. In brief, 1% formaldehyde reagent (Solarbio) was applied to incubate MCF-7 and MDA-MB-231 cells for 10 min under room-temperature conditions to induce crosslinking, and glycine was added to cease this chemical reaction. After lysis, the chromatin was subjected to sonication to generate fragments in the 200–500 bp range. An aliquot was kept for the input control, while the remaining material was incubated with anti-GATA2 antibody or normal rabbit IgG (ab171870, Abcam). After capturing the antibody–protein–DNA complexes with protein A/G magnetic beads, the cross-links were reversed and the DNA was purified, followed by qPCR to measure the enrichment of IER3 promoter fragments that contain the predicted binding sites.

Dual-luciferase reporter assay

GeneChem (Shanghai, China) synthesized and inserted into the pGL3-Basic vector the wild-type (WT-IER3) and mutant (MUT-IER3) promoter segments of IER3 that carry the putative GATA2-binding sites. The pRL-TK Renilla luciferase plasmid (Promega, Madison, WI, USA) was included as an internal standard in the co-transfection mixture with WT-IER3 or MUT-IER3 reporter, oe-GATA2 or control vector, delivered into MCF-7 and MDA-MB-231 cells via Lipofectamine 3000 (Invitrogen). Luciferase activity was determined using the Dual-Luciferase Assay (Promega) after 48 h of incubation, with firefly readings normalized by Renilla activity.

Animal experiments

BALB/c nude female mice (4–6 weeks, 18–20 g) were sourced from SPF (Beijing, China). Twenty-four mice were randomly assigned using a random number table to the sh-NC, sh-GATA2, sh-GATA2+Vector, and sh-GATA2+oe-IER3 groups, with six mice per group. Stably transfected MDA-MB-231 cells corresponding to each group were collected and resuspended in PBS. After receiving a right-flank subcutaneous injection of 2×10^6 cells in 100 μL of PBS, each mouse was monitored weekly. Tumor length (L) and width (W) were determined with a digital caliper, and tumor volume was estimated using the following equation: $V = 0.5 \times L \times W^2$. After 4 weeks from cell implantation, the tumors were excised, weighed, and documented with photographs, following euthanasia of the mice via cervical dislocation under

EARLY ACCESS

deep isoflurane anesthesia. A portion of each tumor was snap-frozen in liquid nitrogen for Western blot and RT-qPCR, whereas the remaining tissue was fixed in 4% paraformaldehyde for immunohistochemical analysis of Ki-67, CD86, and CD206. Procedures that could cause pain or discomfort were performed under anesthesia to minimize animal suffering and stress. All animal experiments complied with the relevant requirements of the Guideline for Ethical Review of Animal Welfare.

Ethical statement

All patients gave their written consent before sample collection, and the study, which was approved by the Research Ethics Committee of Affiliated Tumor Hospital, Xinjiang Medical University (S-2025140), was carried out following the Declaration of Helsinki guidelines. Approval for the animal study protocol was obtained from the Ethics Committee for Animal Research at Affiliated Tumor Hospital, Xinjiang Medical University (No. IACUC-20250426-147). All animal housing, tumor implantation, and tissue collection procedures were conducted in accordance with the 3R principles and the ARRIVE guidelines.

Statistical analysis

At least three independent biological replicates were performed for each experiment. Technical replicates were conducted when applicable, and the data are presented as mean values ± standard deviation (SD). Statistical analyses were performed using GraphPad Prism 9.0 software. For comparisons between two groups, paired or unpaired two-tailed Student's t-tests were used, as appropriate. For comparisons among multiple groups, one-way analysis of variance (ANOVA) was performed, with Tukey's multiple comparison test used for subsequent pairwise comparisons. Two-way ANOVA was used for experiments involving two independent factors. Spearman's rank correlation analysis was used to assess correlations between gene expression levels and between gene expression and immune cell infiltration. A p value < 0.05 was considered statistically significant. Detailed statistical results are provided in Supplementary Table 1 (All statistical results).

RESULTS

Screening of immune-related key genes in BC

To screen immune-related key genes in BC, differential expression analyses were first performed using the GEO bulk transcriptomic datasets GSE10810 and GSE42568. In

the GSE10810 dataset, which included 31 BC tissues and 27 normal breast tissues, 1481 DEGs were identified, including 454 upregulated and 1027 downregulated genes. The volcano plot showed the overall distribution of these genes (Figure 1A). In the GSE42568 dataset, which included 104 BC tissues and 17 normal breast tissues, 3536 DEGs were obtained, including 1791 upregulated and 1745 downregulated genes (Figure 1B). Subsequently, 2869 IRGs were collected from the ImmPort and MSigDB. Intersection of these IRGs with the DEGs identified in the two bulk transcriptomic datasets yielded 228 bulk transcriptome-derived IRGs (Figure 1C). The scRNA-seq dataset GSE161529 was subsequently analyzed to characterize differential expression patterns across cell populations. DEGs were independently identified in B cells (Figure 1D), macrophages (Figure 1E), T cells (Figure 1F), and epithelial cells (Figure 1G), and their overall distributions were visualized using volcano plots. To identify transcriptional alterations shared across multiple TME-associated cell populations, the DEGs from these four major cell types were intersected. Intersection of the DEGs from these four cell populations yielded 179 shared genes, which were used for subsequent candidate-gene screening (Figure 1H). Finally, intersection of GEO-IRG and SC-IRG identified five candidate genes: gamma-aminobutyric acid type A receptor-associated protein-like 1 (GABARAPL1), C-X-C motif chemokine ligand 2 (CXCL2), AT-rich interaction domain 5B (ARID5B), nuclear receptor subfamily 3 group C member 1 (NR3C1), and IER3 (Figure 1I).

Identification of IER3 as a key immune-related gene in BC

To further identify core genes, SVM-RFE analysis was performed using the GSE42568 dataset, and GABARAPL1 and IER3 were identified as two core genes (Figure 2A–B). Considering that both genes represented potential candidates, their biological relevance was further evaluated. Previous studies have reported that GABARAPL1 may exert context-dependent biological functions across different BC subtypes [32, 33]. Meanwhile, correlation analysis indicated that IER3 was more closely associated with immune-cell infiltration characteristics in BC. Therefore, IER3 was selected for subsequent mechanistic investigation. Compared with normal tissues, IER3 was significantly upregulated in BC tissues in the GSE10810 (Figure 2C), GSE42568 (Figure 2D), and TCGA-BRCA datasets (Figure 2E). TIMER2.0 immune-infiltration analysis further showed that IER3 expression was associated with

EARLY ACCESS

the estimated infiltration levels of immune-cell populations, including negative correlations with B-cell (Figure 2F), $CD8^+$ T-cell (Figure 2G), and M1 macrophage infiltration (Figure 2H), but positively correlated with M2 macrophage infiltration (Figure 2I).

IER3 knockdown suppresses malignant phenotypes in BC cells

To validate the expression pattern of IER3 in clinical BC specimens, RT-qPCR and Western blot analyses were performed. IER3 mRNA and protein levels were significantly higher in BC tissues than in paired adjacent non-tumor breast tissues (Figure 3A–B). Consistently, IER3 protein expression was markedly elevated in MCF-7 and MDA-MB-231 cells compared with MCF-10A cells (Figure 3C). To investigate the functional role of IER3 in BC cells, IER3 was silenced in MCF-7 and MDA-MB-231 cells using short hairpin RNA. Western blot confirmed that sh-IER3 markedly reduced IER3 protein expression (Figure 3D). Moreover, IER3 knockdown significantly reduced colony formation (Figure 3E), increased apoptosis (Figure 3F), and impaired cell migration (Figure 3G) and invasion (Figure 3H).

IER3 promotes BC cell-mediated immunosuppression

To determine whether IER3 expression in BC cells regulates $CD8^+$ T-cell function, MCF-7 and MDA-MB-231 cells transfected with sh-NC or sh-IER3 were cocultured with primary human $CD8^+$ T cells. CFSE analysis indicated that IER3 knockdown in BC cells significantly promoted $CD8^+$ T-cell proliferation (Figure 4A–B). Flow-cytometric analysis revealed reduced $CD8^+$ T-cell apoptosis in the sh-IER3 coculture group (Figure 4C). In addition, IFN-γ level in the coculture supernatants was increased after $CD8^+$ T cells were cocultured with IER3-silenced MCF-7 and MDA-MB-231 cells (Figure 4D–E). Subsequently, BC cells were cocultured with M0 macrophages to investigate the effect of IER3 on macrophage polarization. Flow cytometry showed that IER3 knockdown increased the proportion of CD86-positive macrophages while reducing the proportion of CD206-positive macrophages (Figure 4F–G). RT-qPCR further demonstrated that IER3 knockdown increased IL-1β mRNA expression and decreased IL-10 mRNA expression following IER3 knockdown (Figure 4H–I).

GATA2 binds to the IER3 promoter and activates IER3 transcription

To investigate the upstream transcriptional regulatory mechanism of IER3, the JASPAR database was used to predict transcription factor-binding sites within the

IER3 promoter region. GATA2 was predicted to bind to two potential sites in the IER3 promoter, designated Site #1 and Site #2 (Figure 5A). GEPIA analysis further revealed a positive correlation between GATA2 and IER3 expression in BC tissues (Figure 5B). Next, MCF-7 and MDA-MB-231 cells were transfected with sh-GATA2 or oe-GATA2 to silence or overexpress GATA2, respectively. Western blot confirmed the knockdown and overexpression efficiency of GATA2 (Figure 5C). In addition, GATA2 knockdown decreased IER3 mRNA and protein expression, whereas GATA2 overexpression increased IER3 expression (Figure 5D–E). ChIP-qPCR analysis showed that the IER3 promoter fragment was significantly enriched by immunoprecipitation with the anti-GATA2 antibody compared with IgG, indicating that GATA2 binds to the IER3 promoter (Figure 5F). Dual-luciferase reporter assay further demonstrated that GATA2 overexpression enhanced the activity of WT-IER3 promoter reporters containing Site #1 or Site #2 but had no effect on MUT-IER3 reporter activity (Figure 5G–H). Moreover, RT-qPCR and Western blot analyses showed that GATA2 mRNA and protein levels were significantly higher in BC tissues than in normal tissues (Figure 5I–J), and GATA2 protein expression was also elevated in BC cell lines compared with normal mammary epithelial cells (Figure 5K). Furthermore, the associations between GATA2/IER3 expression levels and clinicopathological characteristics were evaluated in 63 BC patients. The results showed that GATA2 and IER3 expression levels were associated with several clinical parameters, including lymph node metastasis and TNM stage (Supplementary Table 2). Correlation analysis further confirmed a significant positive association between GATA2 and IER3 expression in clinical specimens (Figure 5L, $r = 0.5818$, $p < 0.0001$).

IER3 overexpression attenuates the effects of GATA2 knockdown on BC cells and cocultured immune cells

Rescue experiments were subsequently performed to examine whether IER3 overexpression could modify the effects of GATA2 knockdown. Western blot showed that IER3 overexpression restored the reduced IER3 expression induced by GATA2 knockdown (Figure 6A). Functionally, GATA2 knockdown reduced BC cell colony formation (Figure 6B), increased BC cell apoptosis (Figure 6C), and inhibited BC cell migration (Figure 6D) and invasion (Figure 6E). These effects were partially reversed by IER3 overexpression. In the $CD8^+$ T-cell coculture system, IER3 overexpression

EARLY ACCESS

partially reversed the increased $CD8^+$ T-cell proliferation (Figure 6F–G), reduced apoptosis (Figure 6H), and elevated IFN-γ secretion (Figure 6I–J) induced by GATA2 knockdown. In the macrophage coculture system, GATA2 knockdown increased the proportion of CD86-positive macrophages and decreased the proportion of CD206-positive macrophages, whereas IER3 overexpression attenuated these changes (Figure 6K–M). Consistently, RT-qPCR showed that IER3 overexpression reversed the increased interleukin-1 beta mRNA expression and decreased interleukin-10 mRNA expression induced by GATA2 knockdown (Figure 6N–O).

IER3 overexpression attenuates the inhibitory effect of GATA2 knockdown on BC growth in vivo

A nude mouse xenograft model was established by subcutaneously injecting MDA-MB-231 cells from the sh-NC, sh-GATA2, sh-GATA2+Vector, and sh-GATA2+oe-IER3 groups. Compared with the sh-NC group, GATA2 knockdown significantly reduced tumor volume (Figure 7A) and tumor weight (Figure 7B–C). IER3 overexpression partially reversed the inhibitory effect of GATA2 knockdown on tumor growth. Western blot confirmed that GATA2 knockdown decreased GATA2 and IER3 protein expression, whereas IER3 overexpression restored IER3 expression (Figure 7D–E). IHC staining showed that IER3 overexpression was associated with increased Ki67 and CD206 staining and decreased CD86 staining in tumors with GATA2 knockdown (Figure 7F). Consistently, IER3 overexpression reversed the increased IL-1β level and decreased IL-10 level induced by GATA2 knockdown (Figure 7G–H).

DISCUSSION

BC ranks among the top prevalent malignant tumors affecting the female population globally [34, 35], and most BC-related deaths are attributable to tumor metastasis. Metastatic BC remains associated with a poor prognosis despite advances in systemic treatment [36]. Despite considerable advances in BC treatment, tumor metastasis, therapeutic resistance, and treatment-related adverse effects continue to limit clinical benefits [37, 38]. In recent years, immunotherapies have provided new treatment options for advanced cancers [39, 40]. However, therapeutic responses vary considerably among patients with BC, and the underlying mechanisms remain incompletely understood. In this investigation, bulk transcriptomic and scRNA-seq data were integrated with machine learning algorithms to identify IER3 as an

EARLY ACCESS

immune-related candidate gene. The results further demonstrated that the transcription factor GATA2 interacted with the IER3 promoter and enhanced IER3 transcription, thereby promoting the malignant phenotypes of BC cells and generating an immune-suppressive context via attenuation of $CD8^+$ T-cell responses and driving macrophages to an M2-like macrophage-associated marker profile.

The integration of bulk transcriptomics and scRNA-seq has become an important approach for investigating tumor heterogeneity and identifying cell type-specific regulatory networks within the TME [41, 42]. Here, integrative analysis of bulk and single-cell transcriptomic data combined with SVM-RFE identified GABARAPL1 and IER3 as candidate immune-related genes in BC. GABARAPL1, also known as glandular epithelial cell protein 1 (GEC1), is classified as a member of the mammalian ATG8 family and functions in various biological processes, including protein trafficking, autophagy, cell proliferation, and tumor progression [43, 44]. It has been previously reported that GABARAPL1 expression is reduced in BC and various other malignancies, while elevated expression of GABARAPL1 is linked to improved prognosis in BC patients [33, 45]. However, other findings indicated that GABARAPL1 is overexpressed in triple-negative BC and promotes tumor cell proliferation [32], suggesting that its biological functions may depend on the molecular subtype and cellular context of BC. A stress-inducible immediate early response gene, IER3, can be rapidly transcribed in response to various external stimuli without requiring de novo protein synthesis. It is involved in cell proliferation, apoptosis, and stress adaptation [46, 47]. Numerous investigations have shown that IER3 expression is aberrantly regulated in various cancers, and its clinical relevance to progression and prognosis depends on the tumor type [48]. Considering the context-dependent roles of GABARAPL1 across BC subtypes and the previously reported upregulation of IER3 in BC [49], IER3 was chosen for later mechanistic and functional studies.

Bioinformatics and experimental analyses consistently demonstrated that IER3 was overexpressed in BC. Silencing of IER3 suppressed the proliferative, migratory and invasive capacities of BC cells and stimulated apoptotic cell death. Such experimental observations align with the pro-tumor function of IER3 documented in prior BC research [49]. Similarly, IER3 silencing is known to suppress cell viability, migration, and invasion in glioma, while high IER3 expression was linked to T-cell exhaustion-

EARLY ACCESS

associated traits and an immunosuppressive milieu [50]. In the present study, IER3 expression showed an inverse association with the estimated abundances of B cells, $CD8^+$ T cells, and M1-like macrophages, whereas a positive association was observed with M2-like macrophages. The coculture experiments further supported this association, showing that IER3 knockdown in BC cells promoted $CD8^+$ T-cell proliferation and IFN-γ production, reduced $CD8^+$ T-cell apoptosis, and altered CD86, CD206, IL-1β, and IL-10 expression in macrophages.

After establishing the oncogenic and immunomodulatory roles of IER3, the present study further investigated the upstream mechanisms underlying its aberrant expression. The IER3 promoter was scanned for putative transcription factor binding sites via JASPAR, identifying GATA2 as a candidate transcription factor. The zinc-finger transcription factor GATA2 is essential for the development and functioning of multiple organ systems [51, 52]. Dysregulated expression or activity of GATA2 has been linked to the onset and progression of blood cancers as well as diverse solid neoplasms [53, 54]. Earlier reports have indicated that GATA2 might function as a prognostic indicator and a therapeutic agent in BC [55, 56]. However, its direct transcriptional regulation of IER3 and its functional significance within the BC immune microenvironment are still poorly understood. In this study, GATA2 and IER3 were positively correlated and significantly upregulated in BC tissues. Mechanistically, GATA2 enhanced IER3 transcription by binding to its promoter. IER3 overexpression partially counteracted the effects of GATA2 silencing on BC cell phenotypes and cocultured immune-cell responses, supporting a functional association between GATA2 and IER3. Consistently, IER3 overexpression also attenuated the inhibitory effect of GATA2 knockdown on xenograft growth. These findings support a role for the GATA2/IER3 axis in BC progression and suggest its potential involvement in immune regulation.

Limitations

The current study has some limitations. First, the bioinformatics analyses were largely derived from public datasets, and the expression profiles and clinical relevance of GATA2 and IER3 require further validation in larger independent cohorts with comprehensive clinicopathological annotation. Moreover, the clinical samples analyzed in this study were obtained from primary BC specimens at initial diagnosis rather than post-treatment progressive or metastatic lesions. Therefore, the identified

EARLY ACCESS

molecular features may mainly reflect the intrinsic characteristics of primary tumors and may not fully represent acquired alterations associated with therapy resistance. Future studies using paired pre-treatment and post-progression samples are needed to further investigate treatment resistance-related mechanisms. Although SVM-RFE identified both IER3 and GABARAPL1 as core candidate genes, this study selected IER3 for further mechanistic investigation based on its association with immune-related characteristics. GABARAPL1 was not functionally validated in the present study, and its potential role in BC requires further investigation. Second, the scRNA-seq analysis was performed using cell-level differential expression approaches, which may not fully account for the non-independence of cells derived from the same individual and may introduce potential pseudoreplication. Therefore, these findings should be interpreted as exploratory evidence for identifying cell-type-associated molecular patterns rather than definitive patient-level associations. Future studies using patient-level statistical frameworks or larger independent cohorts are warranted. Third, although the in vitro co-culture system provided preliminary evidence regarding tumor–immune cell interactions, it cannot fully reproduce the complex immune microenvironment in vivo. In addition, macrophage responses were evaluated using a limited set of markers, including CD86, CD206, IL-1β, and IL-10, which may not fully reflect macrophage heterogeneity. Fourth, because nude mice exhibit impaired mature T-cell function, the xenograft model mainly reflects the tumor growth-regulatory effects of the GATA2/IER3 axis and cannot adequately evaluate its role in adaptive antitumor immunity, particularly $CD8^+$ T-cell responses. Moreover, CD86/CD206 immunohistochemical staining primarily reflects changes in macrophage-associated marker expression and does not directly demonstrate immune-cell infiltration or macrophage polarization status. Future studies using immunocompetent models combined with quantitative immune profiling are needed to further investigate the immune-related effects of this axis. Finally, although rescue experiments supported a functional relationship between GATA2 and IER3, they were based on ectopic IER3 overexpression and therefore do not directly establish that endogenous IER3 is required for GATA2-mediated biological effects. Further loss-of-function studies combining GATA2 overexpression with endogenous IER3 knockdown are needed to clarify this regulatory dependency. Given the molecular heterogeneity of BC, the biological significance of the GATA2/IER3 axis may vary among different molecular subtypes. Moreover, the therapeutic relevance of targeting

EARLY ACCESS

this axis remains to be established because pharmacological or genetic intervention strategies were not evaluated in the present study. Larger clinical cohorts with detailed treatment information and subtype-specific investigations are warranted to further clarify its clinical significance.

CONCLUSION

GATA2-mediated transcriptional upregulation of IER3 promoted BC cell proliferation, migration, and invasion and was associated with reduced $CD8^+$ T-cell proliferation and IFN-γ secretion, increased $CD8^+$ T-cell apoptosis, and an M2-like macrophage marker profile in the coculture systems (Figure 8). These findings support the involvement of the GATA2/IER3 axis in BC progression and immune-related cellular responses and provide a basis for its further investigation.

Conflicts of interest: Authors declare no conflicts of interest.

Funding: This study was supported by the Natural Science Foundation of Xinjiang Uygur Autonomous Region (2025D01C201).

Data availability: The public datasets analyzed in this study are available from the Gene Expression Omnibus (GEO) database under accession numbers GSE10810, GSE42568, and GSE161529. The processed gene lists generated during the computational analysis, including DEGs, immune-related genes, and overlapping candidate genes, are provided in the supplementary Excel file “Processed gene lists”.

Submitted: 2 September 2026
Accepted: 27 October 2026
Published online: November 23, 2026

EARLY ACCESS

REFERENCES

1. Atasoy O, Anadol E, Yar Saglam AS, Akdemir EY, Coskun YS, Atak E, et al. Synergistic Potential of GLP-1 Receptor Agonists and Radiotherapy in Breast Cancer Treatment: A New Therapeutic Avenue (TROD-GROG 006). Curr Radiopharm. 2025;18(4):318–332. https://doi.org/10.2174/0118744710381356250429045716
2. Iordanishvili E, Bode M, Morscheid S, Lemainque T, Kuhl CK. Breast Cancer Screening: A Decade of Progress. Invest Radiol. 2026;61(3):205–213. https://doi.org/10.1097/rli.0000000000001216
3. Shreya S, Pandey S, Ghosh DK, Puneet, Prasad SB, Grosset CF, et al. Analysis of Endoplasmic Reticulum Stress-Associated Proteins As Prognostic Markers In Breast Cancer. Curr Genomics. 2025;26(6):621–632. https://doi.org/10.2174/0113892029374158251030064845
4. Moura T, Laranjeira P, Caramelo O, Gil AM, Paiva A. Breast Cancer and Tumor Microenvironment: The Crucial Role of Immune Cells. Curr Oncol. 2025;32(3):143. https://doi.org/10.3390/curroncol32030143
5. Liu X, Zhang G, Zhao L. Detection of transmembrane protein 100 in breast cancer: Correlation with malignant progression and chemosensitivity. Cytojournal. 2024;21:65. https://doi.org/10.25259/cytojournal_107_2024
6. Yang F. The integration of radiotherapy with systemic therapy in advanced triple-negative breast cancer. Crit Rev Oncol Hematol. 2024;204:104546. https://doi.org/10.1016/j.critrevonc.2024.104546
7. Liu S, Zhang X, Wang W, Li X, Sun X, Zhao Y, et al. Metabolic reprogramming and therapeutic resistance in primary and metastatic breast cancer. Mol Cancer. 2024;23(1):261. https://doi.org/10.1186/s12943-024-02165-x
8. Villacampa G, Navarro V, Matikas A, Ribeiro JM, Schettini F, Tolosa P, et al. Neoadjuvant Immune Checkpoint Inhibitors Plus Chemotherapy in Early Breast Cancer: A Systematic Review and Meta-Analysis. JAMA Oncol. 2024;10(10):1331–1341. https://doi.org/10.1001/jamaoncol.2024.3456

EARLY ACCESS

9. Zhang Y, Chen H, Mo H, Zhao N, Sun X, Liu B, et al. Distinct cellular mechanisms underlie chemotherapies and PD-L1 blockade combinations in triple-negative breast cancer. Cancer Cell. 2025;43(3):446–463.e7. https://doi.org/10.1016/j.ccell.2025.01.007

10. Nawaz Y, Munir S, Aslam S, Butt FR, Tanvir F, Nawaz B, et al. The Bacterial Role in the Progression of Breast Cancer through Mechanism of Gene Action: Future Prospects with Existing Studies. Curr Genomics. 2025;26(6):458–468. https://doi.org/10.2174/0113892029371937250918105052

11. Harris MA, Savas P, Virassamy B, O'Malley MMR, Kay J, Mueller SN, et al. Towards targeting the breast cancer immune microenvironment. Nat Rev Cancer. 2024;24(8):554–577. https://doi.org/10.1038/s41568-024-00714-6

12. Otterlei Fjørtoft M, Huse K, Rye IH. The Tumor Immune Microenvironment in Breast Cancer Progression. Acta Oncol. 2024;63:359–367. https://doi.org/10.2340/1651-226x.2024.33008

13. Yang L, Hu Q, Huang T. Breast Cancer Treatment Strategies Targeting the Tumor Microenvironment: How to Convert "Cold" Tumors to "Hot" Tumors. Int J Mol Sci. 2024;25(13):7208. https://doi.org/10.3390/ijms25137208

14. Polak R, Zhang ET, Kuo CJ. Cancer organoids 2.0: modelling the complexity of the tumour immune microenvironment. Nat Rev Cancer. 2024;24(8):523–539. https://doi.org/10.1038/s41568-024-00706-6

15. Akinpelu A, Akinsipe T, Avila LA, Arnold RD, Mistriotis P. The impact of tumor microenvironment: unraveling the role of physical cues in breast cancer progression. Cancer Metastasis Rev. 2024;43(2):823–844. https://doi.org/10.1007/s10555-024-10166-x

16. Mou F, Sun Q, Ye Z. Advances in the combination of immunotherapy and radiotherapy for microsatellite-stable metastatic colorectal cancer. Curr Proteomics. 2025;22(5):100049. https://doi.org/10.1016/j.curpro.2025.100049

17. Jiang X, Xu J, Liu M, Xing H, Wang Z, Huang L, et al. Adoptive $CD8^+$ T cell therapy against cancer: Challenges and opportunities. Cancer Lett. 2019;462:23–32. https://doi.org/10.1016/j.canlet.2019.07.017

EARLY ACCESS

18. Farhood B, Najafi M, Mortezaee K. $CD8^+$ cytotoxic T lymphocytes in cancer immunotherapy: A review. J Cell Physiol. 2019;234(6):8509–8521. https://doi.org/10.1002/jcp.27782

19. Tharp KM, Kersten K, Maller O, Timblin GA, Stashko C, Canale FP, et al. Tumor-associated macrophages restrict $CD8^+$ T cell function through collagen deposition and metabolic reprogramming of the breast cancer microenvironment. Nat Cancer. 2024;5(7):1045–1062. https://doi.org/10.1038/s43018-024-00775-4

20. Tang D, Lin S, Zhou J, Lei JH, Shao F, Sun H, et al. Augment proteasome inhibitor efficacy activates $CD8^+$ T cell-mediated antitumor immunity in breast cancer. Cell Rep Med. 2025;6(7):102211. https://doi.org/10.1016/j.xcrm.2025.102211

21. Chu X, Tian Y, Lv C. Decoding the spatiotemporal heterogeneity of tumor-associated macrophages. Mol Cancer. 2024;23(1):150. https://doi.org/10.1186/s12943-024-02064-1

22. Chen D, Zhang X, Li Z, Zhu B. Metabolic regulatory crosstalk between tumor microenvironment and tumor-associated macrophages. Theranostics. 2021;11(3):1016–1030. https://doi.org/10.7150/thno.51777

23. Osipov A, Saung MT, Zheng L, Murphy AG. Small molecule immunomodulation: the tumor microenvironment and overcoming immune escape. J Immunother Cancer. 2019;7(1):224. https://doi.org/10.1186/s40425-019-0667-0

24. Gao J, Liang Y, Wang L. Shaping Polarization Of Tumor-Associated Macrophages In Cancer Immunotherapy. Front Immunol. 2022;13:888713. https://doi.org/10.3389/fimmu.2022.888713

25. Xu J, Ding L, Mei J, Hu Y, Kong X, Dai S, et al. Dual roles and therapeutic targeting of tumor-associated macrophages in tumor microenvironments. Signal Transduct Target Ther. 2025;10(1):268. https://doi.org/10.1038/s41392-025-02325-5

26. Fang W, Zhou T, Shi H, Yao M, Zhang D, Qian H, et al. Progranulin induces immune escape in breast cancer via up-regulating PD-L1 expression on tumor-associated macrophages (TAMs) and promoting $CD8^+$ T cell exclusion. J Exp Clin Cancer Res. 2021;40(1):4. https://doi.org/10.1186/s13046-020-01786-6

EARLY ACCESS

27. Wu E, Zhuo Q, Yin X, Li J, Zhang H, Gu F, et al. Single-cell and bulk transcriptomic analyses reveal PANoptosis-associated immune dysregulation of fibroblasts in periodontitis. Front Immunol. 2025;16:1671919. https://doi.org/10.3389/fimmu.2025.1671919

28. Tan Z, Chen X, Zuo J, Fu S, Wang H, Wang J. Comprehensive analysis of scRNA-Seq and bulk RNA-Seq reveals dynamic changes in the tumor immune microenvironment of bladder cancer and establishes a prognostic model. J Transl Med. 2023;21(1):223. https://doi.org/10.1186/s12967-023-04056-z

29. Fang Z, Li J, Cao F, Li F. Integration of scRNA-Seq and Bulk RNA-Seq Reveals Molecular Characterization of the Immune Microenvironment in Acute Pancreatitis. Biomolecules. 2022;13(1):78. https://doi.org/10.3390/biom13010078

30. Fang K, Ohihoin AG, Liu T, Choppavarapu L, Nosirov B, Wang Q, et al. Integrated single-cell analysis reveals distinct epigenetic-regulated cancer cell states and a heterogeneity-guided core signature in tamoxifen-resistant breast cancer. Genome Med. 2024;16(1):134. https://doi.org/10.1186/s13073-024-01407-3

31. Gong X, Gu L, Yang D, He Y, Li Q, Qin H, et al. Ferroptosis-related genes mediate tumor microenvironment and prognosis in triple-negative breast cancer via integrated RNA-seq analysis. Elife. 2025;13:RP100923. https://doi.org/10.7554/elife.100923

32. Ran L, Hong T, Xiao X, Xie L, Zhou J, Wen G. GABARAPL1 acts as a potential marker and promotes tumor proliferation and metastasis in triple negative breast cancer. Oncotarget. 2017;8(43):74519–74526. https://doi.org/10.18632/oncotarget.20159

33. Berthier A, Seguin S, Sasco AJ, Bobin JY, De Laroche G, Datchary J, et al. High expression of gabarapl1 is associated with a better outcome for patients with lymph node-positive breast cancer. Br J Cancer. 2010;102(6):1024–1031. https://doi.org/10.1038/sj.bjc.6605568

34. Bhatia N, Thareja S. Simulation, 3D-QSAR, molecular docking and pharmacophore mapping studies on indole derivatives as aromatase inhibitors. Lett Drug Des Discov. 2025;22(1):100007. https://doi.org/10.1016/j.lddd.2025.100007

EARLY ACCESS

35. Montazeri Aliabadi H. Molecular Targets for Breast Cancer Therapy. Biomolecules. 2024;14(10):1219. https://doi.org/10.3390/biom14101219

36. Anwar T, Arellano-Garcia C, Ropa J, Chen YC, Kim HS, Yoon E, et al. p38-mediated phosphorylation at T367 induces EZH2 cytoplasmic localization to promote breast cancer metastasis. Nat Commun. 2018;9(1):2801. https://doi.org/10.1038/s41467-018-05078-8

37. Carnevale MG, Colciago RR, De Santis MC, Cortesi L, De Marco C, Marra A, et al. Advancing breast cancer therapy in the era of molecular diagnostics. Breast. 2025;82:104488. https://doi.org/10.1016/j.breast.2025.104488

38. Wu GY, Xiao MZ, Hao WC, Yang ZS, Liu XR, Xu DS, et al. Drug resistance in breast cancer: Mechanisms and strategies for management. Drug Resist Updat. 2025;83:101288. https://doi.org/10.1016/j.drup.2025.101288

39. Ye F, Dewanjee S, Li Y, Jha NK, Chen ZS, Kumar A, et al. Advancements in clinical aspects of targeted therapy and immunotherapy in breast cancer. Mol Cancer. 2023;22(1):105. https://doi.org/10.1186/s12943-023-01805-y

40. Dvir K, Giordano S, Leone JP. Immunotherapy in Breast Cancer. Int J Mol Sci. 2024;25(14):7517. https://doi.org/10.3390/ijms25147517

41. Ding Q, Xu Q, Hong Y, Zhou H, He X, Niu C, et al. Integrated analysis of single-cell RNA-seq, bulk RNA-seq, Mendelian randomization, and eQTL reveals T cell-related nomogram model and subtype classification in rheumatoid arthritis. Front Immunol. 2024;15:1399856. https://doi.org/10.3389/fimmu.2024.1399856

42. Zhao S, Zhang P, Niu S, Xie J, Liu Y, Liu Y, et al. Targeting nucleotide metabolic pathways in colorectal cancer by integrating scRNA-seq, spatial transcriptome, and bulk RNA-seq data. Funct Integr Genomics. 2024;24(2):72. https://doi.org/10.1007/s10142-024-01356-5

43. Beaumont JEJ, Ju J, Barbeau LMO, Demers I, Savelkouls KG, Derks K, et al. GABARAPL1 is essential in extracellular vesicle cargo loading and metastasis development. Radiother Oncol. 2024;190:109968. https://doi.org/10.1016/j.radonc.2023.109968

44. Huang X, Zhou L, Chen J, Zhang S. Targeting GABARAPL1/HIF-2a axis to induce tumor cell apoptosis in nasopharyngeal carcinoma. Iran J Basic Med Sci. 2024;27(2):157–164. https://doi.org/10.22038/ijbms.2023.72952.15863

EARLY ACCESS

45. Nemos C, Mansuy V, Vernier-Magnin S, Fraichard A, Jouvenot M, Delage-Mourroux R. Expression of gec1/GABARAPL1 versus GABARAP mRNAs in human: predominance of gec1/GABARAPL1 in the central nervous system. Brain Res Mol Brain Res. 2003;119(2):216–219. https://doi.org/10.1016/j.molbrainres.2003.09.011

46. He FY, Chen G, He RQ, Huang ZG, Li JD, Wu WZ, et al. Expression of IER3 in hepatocellular carcinoma: clinicopathology, prognosis, and potential regulatory pathways. PeerJ. 2022;10:e12944. https://doi.org/10.7717/peerj.12944

47. Dou Q, Tong H, Chen J, Yi X, Bai L, He J, et al. IER3 drives the transition from sepsis-associated AKI to CKD by suppressing the mitochondrial translocation of PRDX5. Cell Mol Life Sci. 2025;82(1):439. https://doi.org/10.1007/s00018-025-05963-8

48. Kanduri M, Subhash S, Putino R, Mahale S, Kanduri C. IER3: exploring its dual function as an oncogene and tumor suppressor. Cancer Gene Ther. 2025;32(4):450–463. https://doi.org/10.1038/s41417-025-00891-y

49. Böckers M, Paul NW, Efferth T. Bisphenolic compounds alter gene expression in MCF-7 cells through interaction with estrogen receptor α. Toxicol Appl Pharmacol. 2020;399:115030. https://doi.org/10.1016/j.taap.2020.115030

50. Wang Q, Zhang C, Pang Y, Cheng M, Wang R, Chen X, et al. Comprehensive analysis of bulk, single-cell RNA sequencing, and spatial transcriptomics revealed IER3 for predicting malignant progression and immunotherapy efficacy in glioma. Cancer Cell Int. 2024;24(1):332. https://doi.org/10.1186/s12935-024-03511-1

51. Jung MM, Tran VL, Xiong Y, Johnson KD, Katsumura KR, Liu P, et al. GATA2 decommissioning of enhancers: A mechanism to constrain inflammatory signaling. Cell Rep. 2025;44(10):116344. https://doi.org/10.1016/j.celrep.2025.116344

52. Jackson-Strong M, Ganguly S, Francis A, Rago F, Kanshana J, Michalides BA, et al. GATA2 controls alveolar macrophage inflammatory gene expression and metabolic function. JCI Insight. 2026;11(7):e196246. https://doi.org/10.1172/jci.insight.196246

EARLY ACCESS

53. Polaki US, Gilpin TE, Patil AT, Chiu E, Baker R, Liu P, et al. Loss of GATA2 promotes invasion and predicts cancer recurrence and survival in uterine serous carcinoma. JCI Insight. 2025;10(9):e187073. https://doi.org/10.1172/jci.insight.187073

54. Jin Z, Wang H, Tang R, Pan B, Lee HJ, Liu S, et al. GATA2 promotes castration-resistant prostate cancer development by suppressing IFN-β axis-mediated antitumor immunity. Oncogene. 2024;43(34):2595–2610. https://doi.org/10.1038/s41388-024-03107-z

55. Tan C, Lyu H, Ruan S, Wu Y, Larsen ME, Tang SC, et al. Subtype-specific HER3 enrichment in basal-like breast cancer is regulated via the GATA2/GATA3-FOXA1 axis. Cancer Lett. 2025;633:218001. https://doi.org/10.1016/j.canlet.2025.218001

56. Erceylan ÖF, Savaş A, Göv E. Targeting the tumor stroma: integrative analysis reveal GATA2 and TORYAIP1 as novel prognostic targets in breast and ovarian cancer. Turk J Biol. 2021;45(2):127–137. https://doi.org/10.3906/biy-2010-39

EARLY ACCESS

TABLES AND FIGURES WITH LEGENDS

Table 1. Primer sequences used for reverse transcription-quantitative PCR.

Primer name	Primer sequence (5′–3′)
GATA2 (human)-F	GTGAGCCCCTTCTCCAAGAC
GATA2 (human)-R	AAAAGGTGGGAGCCAGAGTG
IER3 (human)-F	TCCTGATGGCTGAAGAGGGT
IER3 (human)-R	ATTAAAGGGCTCGAGGACGG
IL1β (human)-F	CCAGCTACGAATCTCCGACC
IL1β (human)-R	CATGGCCACAACAACTGACG
IL10 (human)-F	CGAGATGCCTTCAGCAGAGT
IL10 (human)-R	CGCCTTGATGTCTGGGTCTT
IL1β (mouse)-F	ATGCCACCTTTTGACAGTGATG
IL1β (mouse)-R	TGTGCTGCTGCGAGATTTGA
IL10 (mouse)-F	ACCTGGTAGAAGTGATGCCC
IL10 (mouse)-R	ACACCTTGGTCTTGGAGCTTAT
GAPDH (mouse)-F	GGAGAGTGTTTCCTCGTCCC
GAPDH (mouse)-R	ATGAAGGGGTCGTTGATGGC
GAPDH (human)-F	GTCAAGGCTGAGAACGGGAA
GAPDH (human)-R	AAATGAGCCCCAGCCTTCTC

Abbreviations**:** F, forward; GAPDH, glyceraldehyde-3-phosphate dehydrogenase; GATA2, GATA binding protein 2; IER3, immediate early response 3; IL, interleukin; R, reverse; RT-qPCR, reverse transcription-quantitative polymerase chain reaction.

EARLY ACCESS

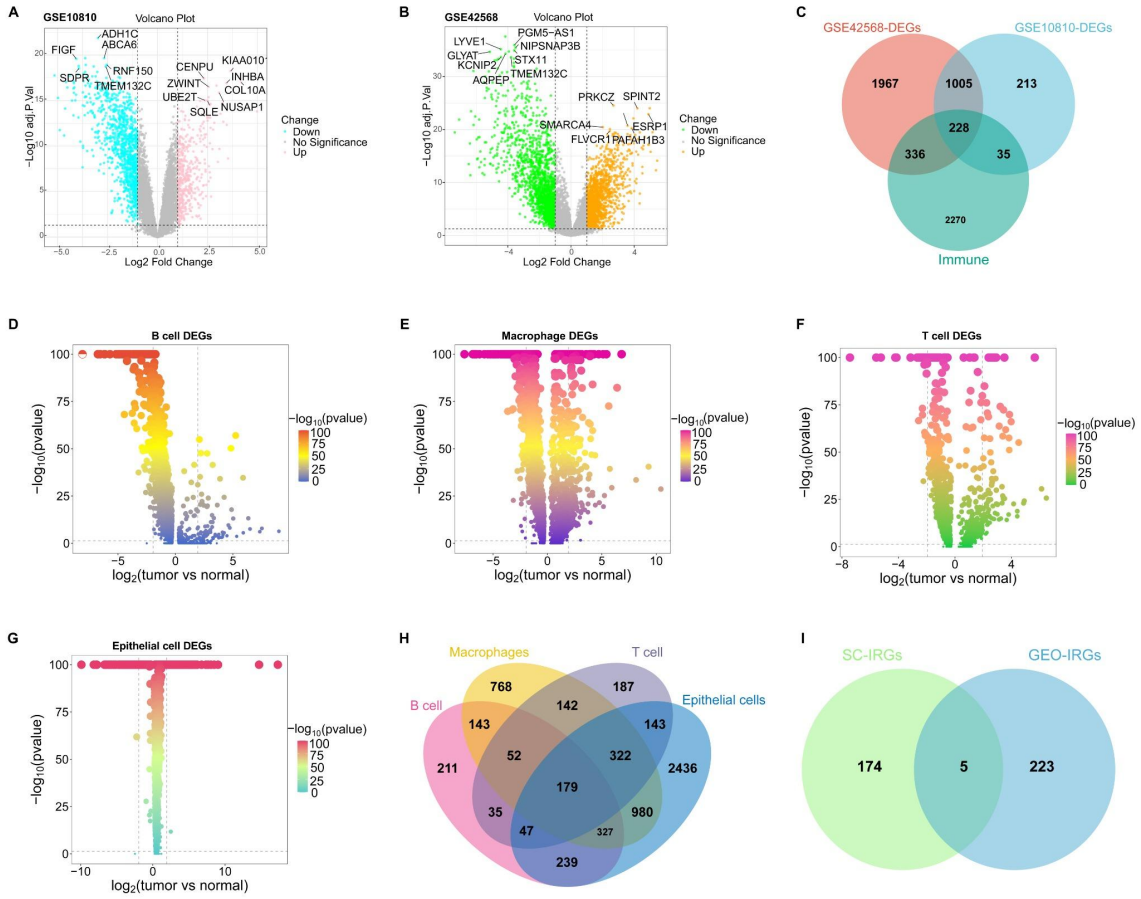


Figure 1. Screening of immune-related candidate genes in breast cancer. (A, B) Volcano plots of differentially expressed genes (DEGs) in GSE10810 (31 tumor and 27 normal samples) and GSE42568 (104 tumor and 17 normal samples), respectively. **(C)** Overlap between the two DEG sets and immune-related genes from ImmPort and MSigDB. **(D–G)** Volcano plots of DEGs between tumor and normal samples in B cells, macrophages, T cells, and epithelial cells, respectively, in GSE161529. **(H)** Overlap of DEGs across these four cell populations. **(I)** Overlap between SC-IRGs and GEO-IRGs. **Abbreviations:** DEG, differentially expressed gene; GEO, Gene Expression Omnibus; GEO-IRG, GEO-derived immune-related candidate gene; ImmPort, Immunology Database and Analysis Portal; IRG, immune-related gene; MSigDB, Molecular Signatures Database; SC-IRG, single-cell-derived immune-related candidate gene.

EARLY

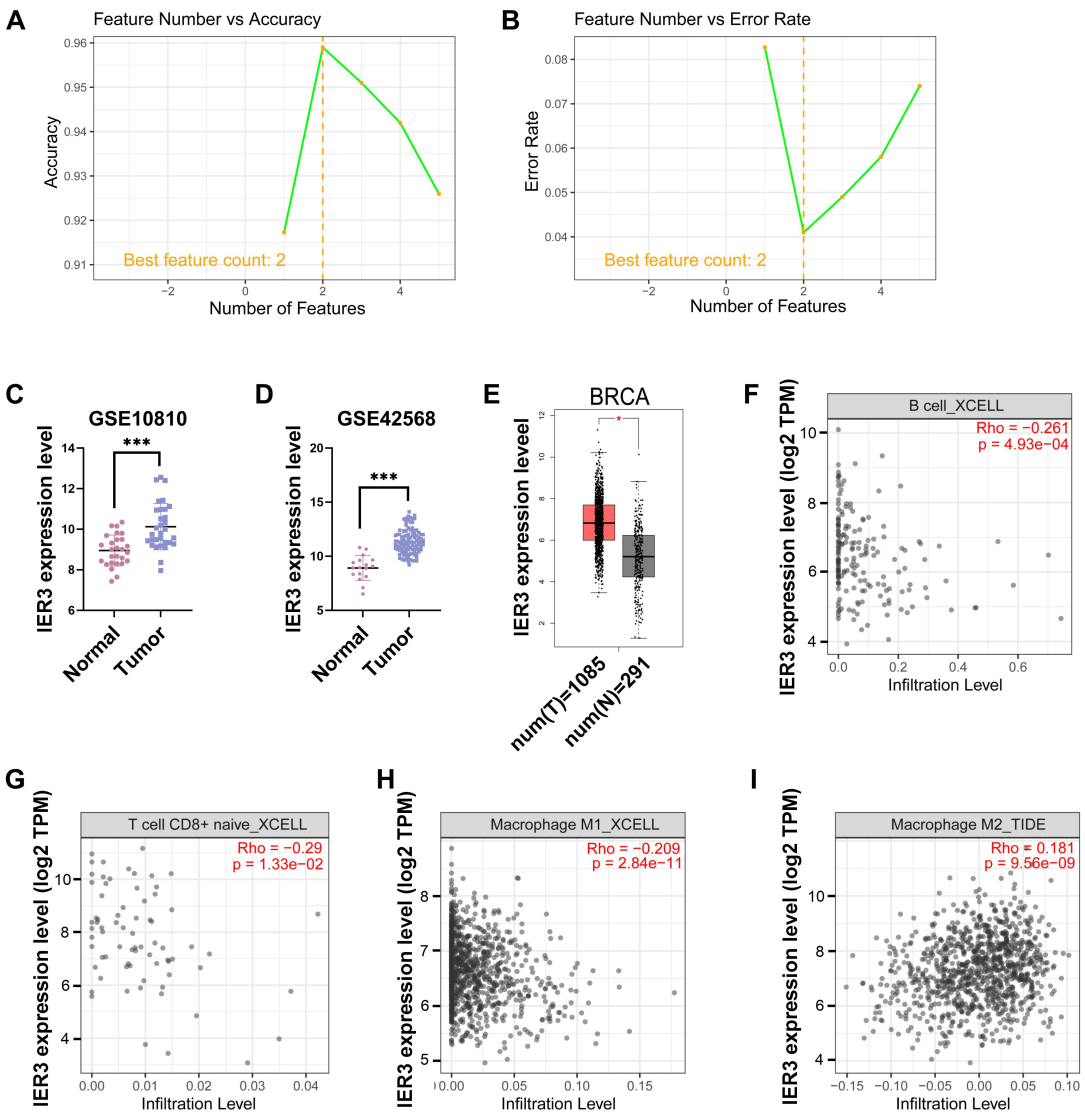


Figure 2. Identification of IER3 as a key immune-related gene in breast cancer. **(A, B)** Classification accuracy and error rate for different feature counts in the SVM-RFE analysis of GSE42568. The selected feature count was two. **(C–E)** IER3 expression in tumor and normal tissues in GSE10810, GSE42568, and the TCGA-BRCA analysis, respectively. **(F–I)** Associations between IER3 expression and estimated infiltration levels of B cells, naive $CD8^+$ T cells, M1 macrophages, and M2 macrophages, respectively, assessed using TIMER2.0. Panels F–H are labeled XCELL and panel I is labeled TIDE in the supplied figure. $*p < 0.05$, $***p < 0.001$. **Abbreviations:** BRCA, breast invasive carcinoma; IER3, immediate early response 3; SVM-RFE, support vector machine-recursive feature elimination; TCGA, The Cancer Genome Atlas; TIDE, Tumor Immune Dysfunction and Exclusion; TIMER, Tumor Immune Estimation Resource.

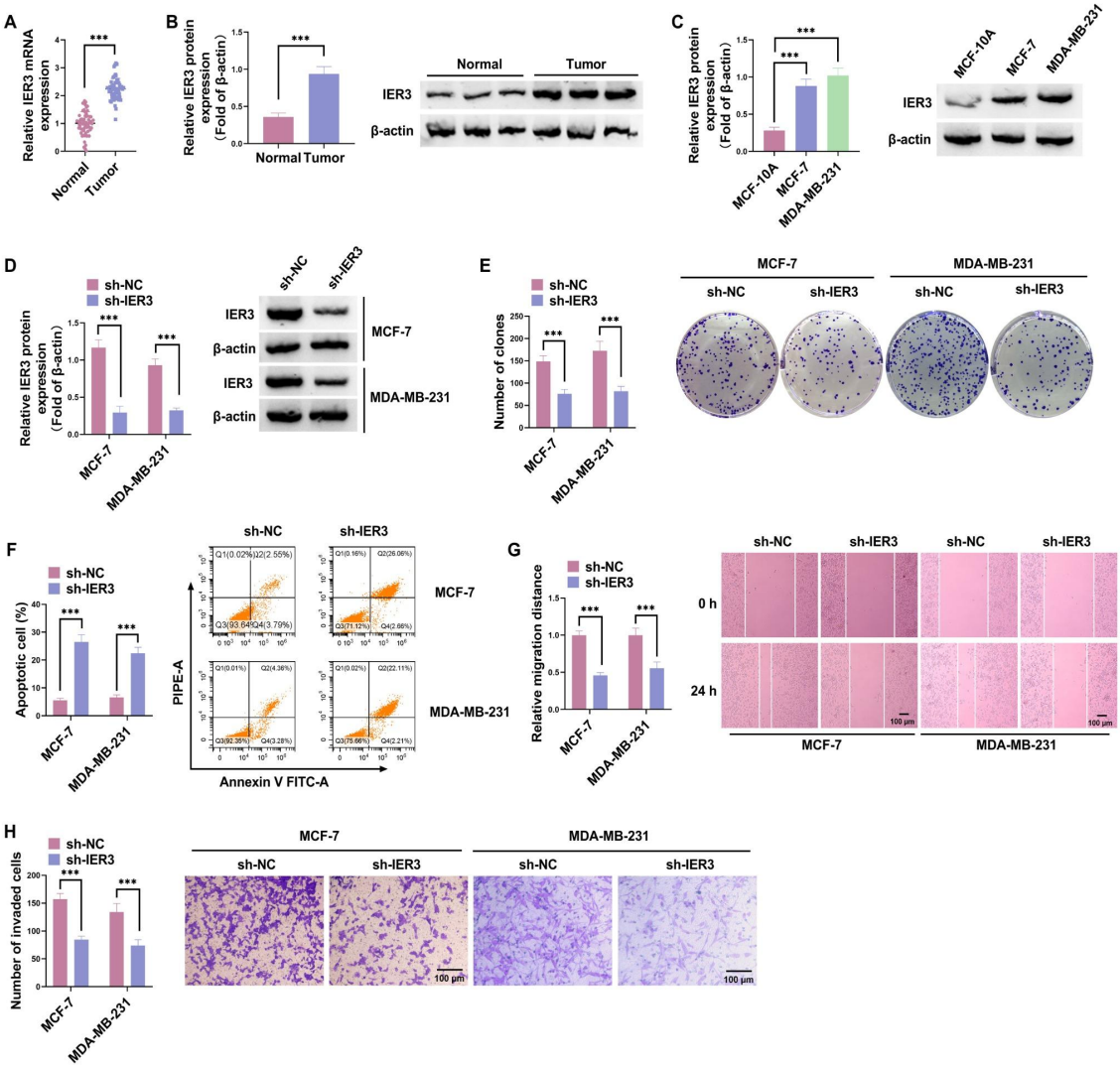


Figure 3. IER3 knockdown suppresses malignant phenotypes in breast cancer cells. (A) IER3 mRNA expression measured by RT-qPCR in 63 paired breast cancer and adjacent non-tumor tissue samples. **(B)** Western blot analysis of IER3 protein expression in tumor and non-tumor tissues (n = 3). **(C)** IER3 protein expression in MCF-10A, MCF-7, and MDA-MB-231 cells. **(D–H)** MCF-7 and MDA-MB-231 cells were transfected with sh-NC or sh-IER3. **(D)** IER3 protein expression. **(E)** Colony formation. **(F)** Apoptosis measured by flow cytometry. **(G)** Migration measured by wound-healing assay at 0 and 24 h. **(H)** Invasion measured by Transwell assay. Scale bars: 100 μm in G and H. Data are presented as mean ± SD. ***p < 0.001. **Abbreviations:** FITC, fluorescein isothiocyanate; IER3, immediate early response 3; PI, propidium iodide; RT-qPCR, reverse transcription-quantitative polymerase chain

reaction; SD, standard deviation; sh-IER3, short hairpin RNA targeting IER3; sh-NC, negative-control short hairpin RNA.

EARLY ACCESS

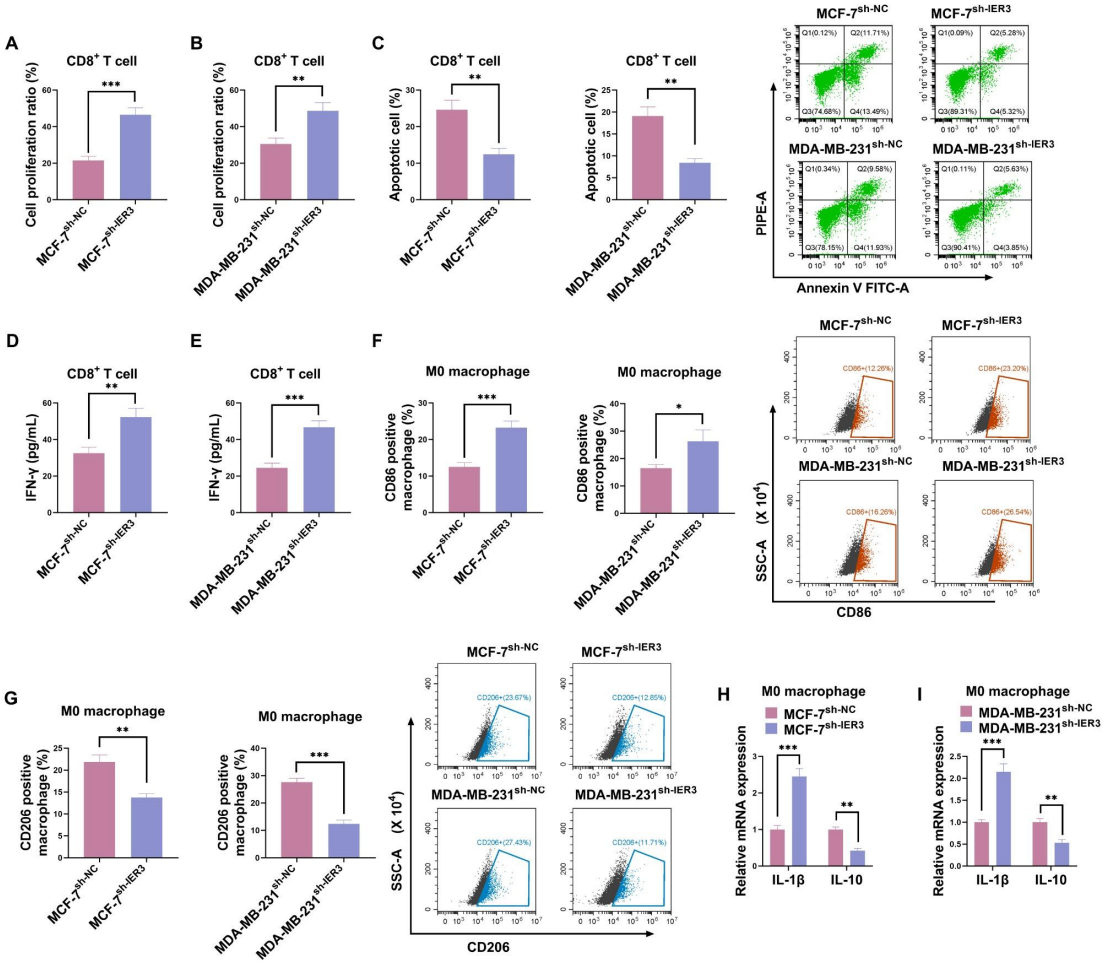


Figure 4. IER3 promotes breast cancer cell-mediated immunosuppression. MCF-7 and MDA-MB-231 cells transfected with sh-NC or sh-IER3 were cocultured with primary human CD8$^+$ T cells or M0-like macrophages. **(A, B)** CD8$^+$ T-cell proliferation measured by CFSE dilution after coculture with MCF-7 and MDA-MB-231 cells, respectively. **(C)** CD8$^+$ T-cell apoptosis measured by flow cytometry. **(D, E)** IFN-γ concentrations in the corresponding coculture supernatants. **(F, G)** Proportions of CD86-positive and CD206-positive macrophages, respectively. **(H, I)** IL-1β and IL-10 mRNA expression in macrophages cocultured with MCF-7 and MDA-MB-231 cells, respectively. Data are presented as mean ± SD. *$p < 0.05$, **$p < 0.01$, ***$p < 0.001$. **Abbreviations:** CD, cluster of differentiation; CFSE, carboxyfluorescein succinimidyl ester; FITC, fluorescein isothiocyanate; IER3, immediate early response 3; IFN-γ, interferon gamma; IL, interleukin; PI, propidium iodide; SD, standard deviation; sh-IER3, short hairpin RNA targeting IER3; sh-NC, negative-control short hairpin RNA; SSC-A, side-scatter area.

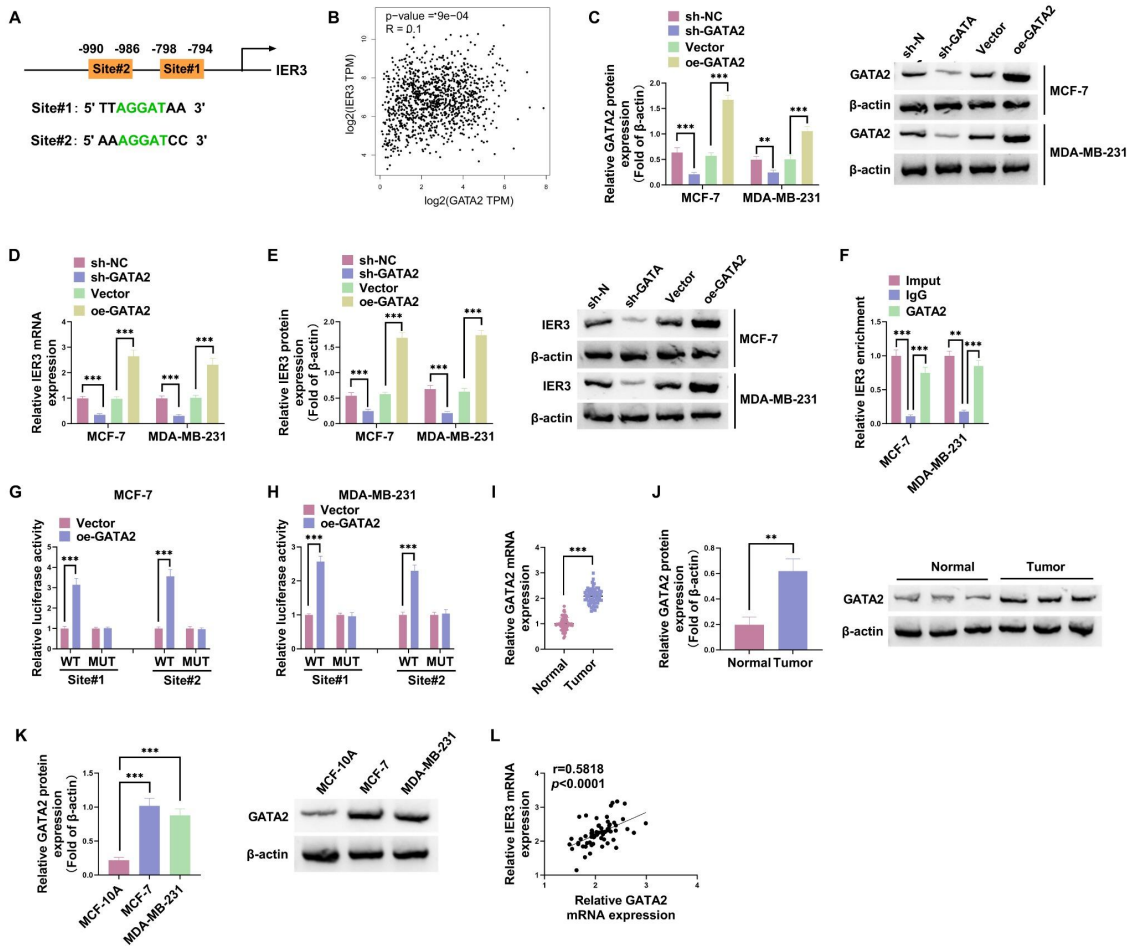


Figure 5. GATA2 binds to the IER3 promoter and activates IER3 transcription. **(A)** Predicted GATA2-binding sites in the IER3 promoter. **(B)** Association between GATA2 and IER3 expression in the GEPIA analysis. **(C)** GATA2 protein expression after GATA2 knockdown or overexpression. **(D, E)** IER3 mRNA and protein expression in the same treatment groups. **(F)** ChIP-qPCR analysis of GATA2 binding to the IER3 promoter, with input and IgG controls. **(G, H)** Luciferase activity of wild-type and mutant promoter reporters in MCF-7 and MDA-MB-231 cells, respectively. **(I)** GATA2 mRNA expression in 63 paired tumor and adjacent non-tumor samples. **(J)** GATA2 protein expression in tumor and non-tumor tissues (n = 3). **(K)** GATA2 protein expression in MCF-10A, MCF-7, and MDA-MB-231 cells. **(L)** Correlation between GATA2 and IER3 mRNA expression in clinical samples (r = 0.5818, p < 0.0001). Data are presented as mean ± SD where applicable. **p < 0.01, ***p < 0.001. **Abbreviations:** ChIP-qPCR, chromatin immunoprecipitation-quantitative polymerase chain reaction; GATA2, GATA binding protein 2; GEPIA, Gene Expression Profiling Interactive Analysis; IER3, immediate early response 3; IgG, immunoglobulin G; MUT, mutant; oe-GATA2, GATA2 overexpression; SD, standard deviation; sh-

GATA2, short hairpin RNA targeting GATA2; sh-NC, negative-control short hairpin RNA; TPM, transcripts per million; WT, wild type.

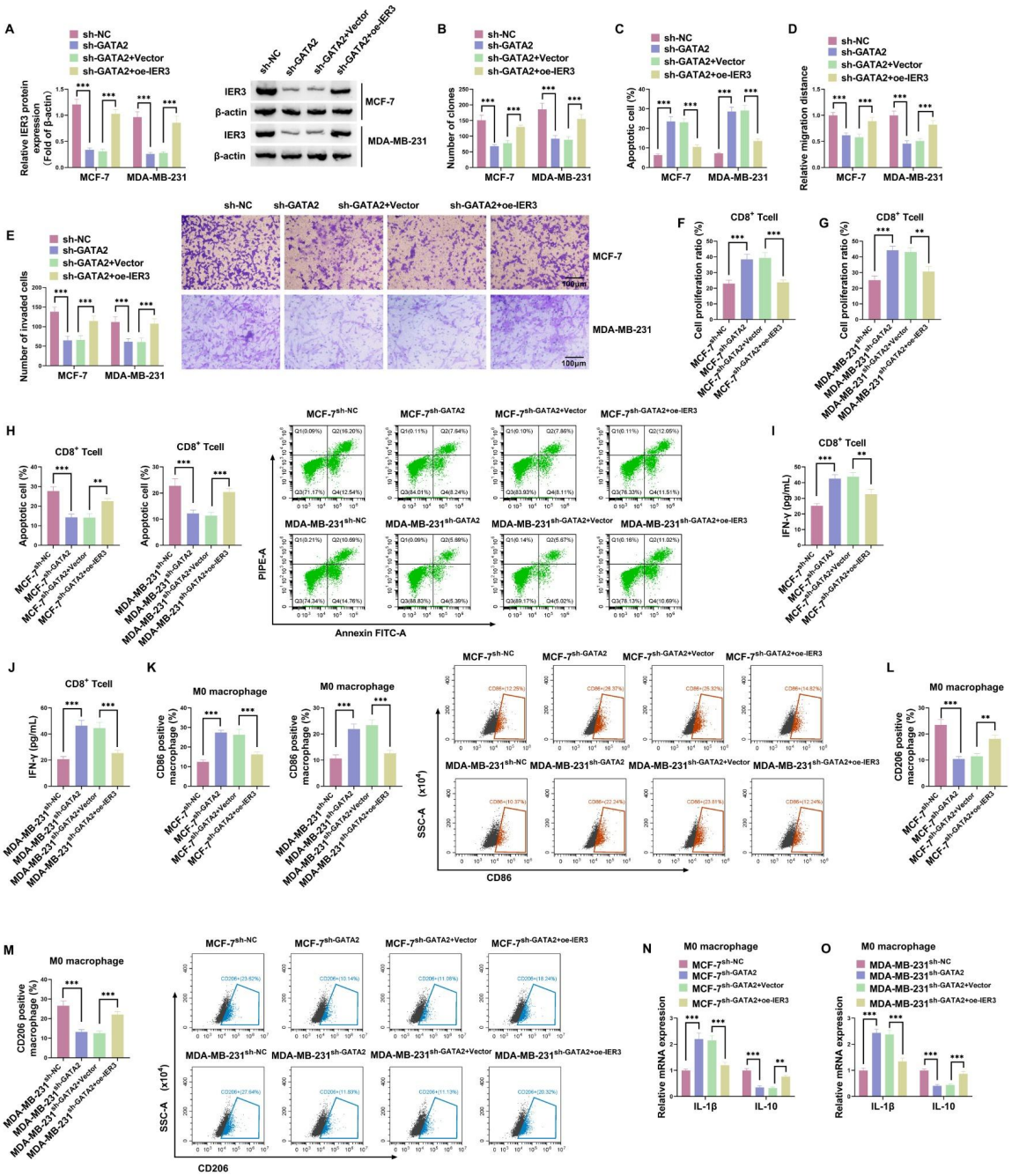


Figure 6. IER3 overexpression attenuates the effects of GATA2 knockdown on breast cancer cells and cocultured immune cells. MCF-7 and MDA-MB-231 cells were assigned to sh-NC, sh-GATA2, sh-GATA2 + Vector, or sh-GATA2 + oe-IER3 groups. **(A)** IER3 protein expression. **(B)** Colony formation. **(C)** Breast cancer cell apoptosis. **(D)** Migration assessed by wound-healing assay. **(E)** Invasion assessed by

Transwell assay; scale bars, 100 μm. **(F, G)** $CD8^+$ T-cell proliferation after coculture with MCF-7 or MDA-MB-231 cells, respectively. **(H)** $CD8^+$ T-cell apoptosis. **(I, J)** IFN-γ concentrations in the corresponding coculture supernatants. **(K)** Proportions of CD86-positive macrophages. **(L, M)** Proportions of CD206-positive macrophages following coculture with MCF-7 or MDA-MB-231 cells, respectively. Representative flow-cytometry plots accompany the corresponding quantifications. **(N, O)** IL-1β and IL-10 mRNA expression in macrophages cocultured with MCF-7 or MDA-MB-231 cells, respectively. Data are presented as mean ± SD. $^{**}p < 0.01$, $^{***}p < 0.001$. **Abbreviations:** CD, cluster of differentiation; FITC, fluorescein isothiocyanate; GATA2, GATA binding protein 2; IER3, immediate early response 3; IFN-γ, interferon gamma; IL, interleukin; oe-IER3, IER3 overexpression; PI, propidium iodide; SD, standard deviation; sh-GATA2, short hairpin RNA targeting GATA2; sh-NC, negative-control short hairpin RNA; SSC-A, side-scatter area.

EARLY ACCESS

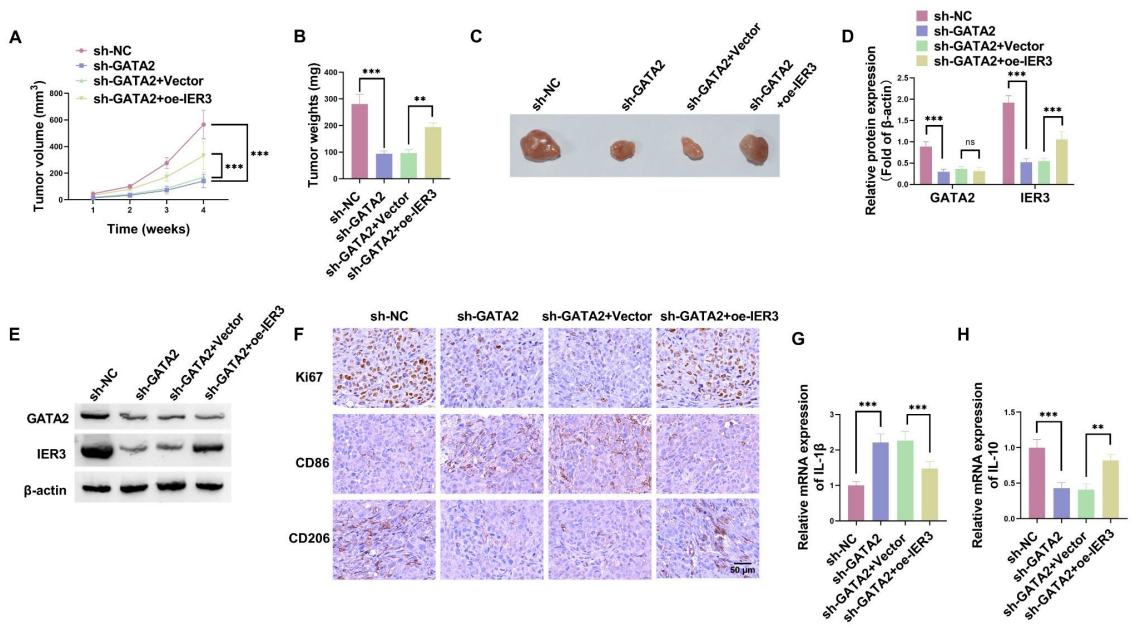


Figure 7. IER3 overexpression attenuates the inhibitory effect of GATA2 knockdown on breast cancer growth *in vivo*. MDA-MB-231 cells from the sh-NC, sh-GATA2, sh-GATA2 + Vector, and sh-GATA2 + oe-IER3 groups were injected subcutaneously into nude mice (2×10^6 cells per mouse; six mice per group). **(A)** Tumor volume over four weeks. **(B)** Tumor weight at the endpoint. **(C)** Representative excised tumors. **(D, E)** Quantification and representative western blots of GATA2 and IER3 protein expression. **(F)** Immunohistochemical staining for Ki-67, CD86, and CD206; scale bar, 50 μm. **(G, H)** IL-1β and IL-10 mRNA expression in tumor tissues, respectively. Data are presented as mean ± SD. ns, not significant; $^{**}p < 0.01$, $^{***}p < 0.001$. **Abbreviations:** CD, cluster of differentiation; GATA2, GATA binding protein 2; IER3, immediate early response 3; IL, interleukin; oe-IER3, IER3 overexpression; SD, standard deviation; sh-GATA2, short hairpin RNA targeting GATA2; sh-NC, negative-control short hairpin RNA.

DRAFT

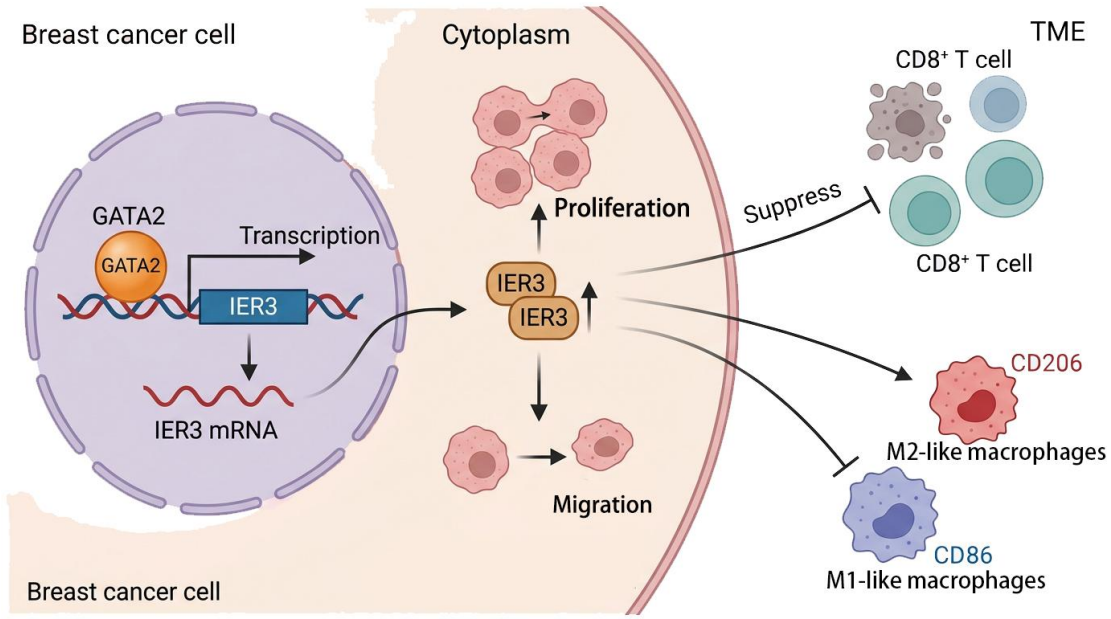


Figure 8. Proposed role of the GATA2/IER3 axis in breast cancer progression and immune-related cellular responses. GATA2 binds to the IER3 promoter and increases IER3 transcription. The experimental findings associate this axis with breast cancer cell proliferation and migration, reduced $CD8^+$ T-cell responses, and changes in macrophage-associated markers. The schematic summarizes findings from the experimental systems used; it does not establish adaptive immune effects in vivo or directly demonstrate macrophage polarization in xenografts. **Abbreviations:** CD, cluster of differentiation; GATA2, GATA binding protein 2; IER3, immediate early response 3; TME, tumor microenvironment.

EARLY ACCESS

SUPPLEMENTAL DATA

Supplemental data are available at the following link:

www.bjbms.org/ojs/index.php/bjbms/article/download/14970/5478

EARLY ACCESS